Arabian Sea Surface Winds and Ocean Transports Determined From ERS-1 Scatterometer

David Halpern

Earth and Space Sciences Division

Jet Propulsion Laboratory

California Institute of Technology

Pasadena, CA 91109

Michael H. Freilich

College of Oceanic and Atmospheric Sciences

Oregon State University

Corvallis, OR 97331

Robert A. Weller

Department of Physical Oceanography

Woods Hole Oceanographic Institution

Woods Hole, MA 02543

Abstract. Satellite scatterometer wind velocity measurements area new source of data for studies of seasonal-to-interannual oeean-atmosphere interactions in the Arabian Sea, where the largest and steadiest wind speeds occur in northern summer. Three satellite wind velocity data products (named CMOD4, FD and IFR2), all created from radar backscatter measured by the first European Remote Sensing Satellite (ERS-1), were compared to moored-buoy wind measurements recorded in the central Arabian Sea during October 1994 to October 1995. Orthogonal regression analysis of 74 collocations indicated IFR2 winds were more representative of buoy winds compared to CMOD4 and FD. IFR2 winds during 1995 are described, including the time of monsoon onset and the path of the Somali Jet. Monthly mean vertical transport across the bottom of the Ekman layer of the Arabian Sea north of 8"N, meridional Ekman transport along 8.5°N, and Sverdrup transport along 8.5° were computed with IFR2 data from May 1992- May 1996. During the 1992-1995 June - September southwest monsoon, upwelling into the Ekman layer of the Arabian Sea occurred at a mean rate of 3.4 Sv (1 Sv = 10^6 m^3 S-l), which was one-third smaller than the volume transport exiting within the Ekman layer across the southern boundary of the Arabian Sea, and the southward Sverdrup transport was 15 Sv. During the 1992- 1996 December - March northeast monsoon, nearly 5 Sv sank below the bottom of the Ekman layer, 4 Sv entered the Arabian Sea in the Ekman layer, and the Sverdrup transport was negligible. Year-to-year transport variations were small.

1. Introduction

Knowledge of spatial variations of vector surface wind stress is critical to understand, model, and predict ocean circulation processes and biological-physical interactions in the Indian Ocean where seasonally reversing winds or monsoons are caused by differential heating of ocean and land. The coupled atmosphere-land-ocean system of the monsoon is one of Earth's most complex phenomena. In Northern Hemisphere summer the wind over the Arabian Sea is dominated by the Somali Jet. Wind direction over the Arabian Sea is southwesterly (towards the northeast) during the June - September southwest monsoon and northeasterly (towards the southwest) during the

December - March northeast monsoon. July wind stress in the Arabian Sea is 2-3 times larger than that in January. Arabian Sea currents are highly sensitive to surface wind stress. *Knox [1987]* provided a good primer on the richness and uniqueness of wind-driven ocean circulations in the North Indian Ocean.

Surface wind stress curl produces a vertical velocity at the bottom of the Ekman layer, which causes water to upwell and sink and which significantly influences large-scale ocean circulation, sea surface temperature, arid near-surface phytoplankton biomass. Wind stress is extremely difficult to measure over the ocean. Therefore, a parametrization of surface wind stress is normally formulated from near-surface wind velocity components [*Trenberth et al., 1990]*. Near-surface wind speed and direction are routinely observed by ships and buoys, inferred from satellite scatterometer measurements, and simulated from atmospheric general circulation models. Of the three wind-measuring techniques, the satellite method is the newest. The coverage, resolution, all-weather capability, and ability to infer wind direction as well as speed make spaceborne scatterometers particularly appealing sources of surface wind velocity for air-sea interaction studies in monsoon regions. Except for three months in 1978, satellite measurements of surface wind velocity did not exist until July 1991 when the European Space Agency (ESA) first European Remote-Sensing Satellite (ERS-1) was launched.

ERS- 1 measures microwave radar backscatter, from which near-surface wind velocity is determined. Typically, four possible wind vectors are retrieved for the same location, and selection of a unique direction is difficult because of symmetries in the model function and the scatterometer measurement geometry [*Naderi et al.*, 1991]. Three ERS - 1 surface wind velocity data products, all created from backscatter measurements provided by ESA, are compared to moored buoy wind observations in the central Arabian Sea to select a data set for analysis. The selected data product is used to compute vertical transport across the bottom of the Ekman layer over the Arabian Sea and Sverdrup and meridional Ekman transports along the southern boundary of the Arabian Sea for 1992- 1996. Results demonstrate the utility of scatterometer data for monsoon ocean-atmosphere response studies.

2. Instrumentation

2.1. IMET

Weller [1996] deployed a surface mooring at 15.5°N, 61.5"E (Figure 1) with an Improved Meteorological (IMET) instrument to measure wind speed and direction at 1-rein intervals at 2.9-m height. Accuracies of I MET wind speed and direction measurements were 5% and 10°, respectively [*Weller and Anderson, 1996)]* I MET was located near the axis of the Somali Jet. IMET data were referenced to IO-m height, assuming neutral atmospheric stratification, logarithmic wind profile, von Karman constant of 0.4, and drag coefficient dependent on wind speed according to that specified by *Trenberth et al. [1990].* At low wind speeds, an error may have been introduced in I MET 10-m height wind estimate by assumption of neutral stratification and neglect of stratification-dependent corrections to the logarithmic profile.

For comparison with ERS - 1 data, arithmetic means of sixty 1-minute IMET values of east-west component (u, positive eastward), north-south component (v, positive northward), and scalar speed were computed. The 1-hour average wind direction was calculated from l-hour *u* and v components. The midpoint of 1-hour averaged 1 MET wind speed and direction was centered at the time of ERS - 1 overflight. The choice of 1 hour to create I MET collocated data was reasonable during the southwest monsoon when the displacement of an air parcel in 1 hour was comparable to the 50-km diameter of the circular region associated with ERS- 1 data.

2.2. ERS-1

The ERS- 1 Active Microwave instrument (AM I) [*Attema*, 1991] was designed to operate either as a synthetic aperture radar or as a wind scatterometer. In wind scatterometer mode, the AMI C-band (5.3 GHz), vertically polarized backscatter cross-section measurements were made in a single 500-km wide swath using three fan-beam antennas oriented at 45,90, and 135 degrees relative to the spacecraft subtrack. Each raw backscatter measurement had a characteristic dimension of 50-70 km. Ground-based data processing produced normalized radar cross-section measurements from each antenna on an approximate 25 km x 25 km along-track/across-track grid

throughout the swath. At the moderate incidence angles characteristic of the ERS-1 measurement swath, backscatter from the ocean surface results primarily from a two-scale resonant scattering mechanism. The calculated normalized radar cross-section of the sea surface is thus a function of both the amplitudes and the directional distributions (relative to the antenna azimuth) of centrimetric-scale surface roughness elements. Wind created centrimetric surface waves, and wind and waves were in equilibrium. Collocated backscatter measurements were used to estimate both wind speed and wind direction [Nader-i *et al.,* 1991].

Three ERS-110-m height wind velocity data sets were used: CMOD4 [*Offiler*, 1994; *Stoffelen and Anderson, 1997];* FD [*Freilich and Dunbar, 1993; Freilich, 1994]; IFR2 [Quilfen and Bentamy,* 1994]. All employed the same back scatter cross-section measurements provided by ESA. Each retrieved winds used a different empirical model function. A model or transfer function relates radar backscatter measurements, incidence angle, radar frequency, radar polarization, and wind speed and direction. A unique physically-based model function cannot be constructed because of insufficient understanding of radar scattering from a wind-generated centimeter-scale sea surface. The CMOD4, FD, and IFR2 model functions, respectively, used November 1991 European Center for Medium-Range Weather Forecasts (ECMWF) wind anal yses, February 1992 National Centers for Environmental Prediction wind analyses, and March - June 1992 National Oceanic and Atmospheric Administration moored-buoy wind measurements. Each used a different algorithm to select a unique wind vector from the (typically four) possible solutions derived from the initial wind retrieval processing. Importantly, no model function nor numerical scheme employed IMET data. Each of the data sets corresponded to estimates of 10 m equivalent neutral stability winds. Errors in the FD model function resulted in an anomalously large number of low speeds [*Graber et aL, 1996]* and, thus, all FD data with wind speeds less than 1.2 m s^{-1} were discarded prior to comparisons with IMET measurements.

Comparisons between IMET measurements and spatially and temporally collocated ERS- 1 wind velocity estimates were used to assess the accuracy and representativeness of the ERS - 1 data sets and to select a single scatterometer product for further analysis. Only ERS - 1 wind vectors

located within 12.5 km of the buoy were included in the comparisons, yielding 74 collocations spanning the time interval 24 October 1994-15 October 1995. The range of I MET collocated wind speeds was 3 to 15 m S-*. The comparison test is noteworthy because of the large percentage of buoy wind speeds greater than 10 m S-l. The mean collocated IMET wind speed was 7.6 m s^{-1}, which is approximately the same as the mean global ocean wind speed. Forty-four (30) collocations were associated with I MET wind speeds below (above) 7.6 m S-l.

IMET measurements are assumed to have fewer errors than ERS-1 data. Moored-buoy wind speed measurements are not error free, as illustrated by *Large et al. [1995],* who identified significant wave-induced biases in 10-m wind speeds computed from buoy measurements recorded within a few meters of the surface. They found altitude-corrected wind speeds to be systematically biased low for true 10-m wind speeds exceeding a transition speed of 7-10 m s^{-1}, depending on anemometer height, because surface waves caused a distortion in the wind profile. Such biases in buoy data would lead to a significant negative slope in the linear regression analysis between IMET minus ERS- 1 residual speed versus IMET wind speed if the ERS-1 data were, in fact, representative of the 10-m wind speed and the collocated data contained a high percentage of high speeds, as in the present case.

Mean IMET minus ERS-1 wind speed residuals were 0.0,0.5, and 0.6 m s^{-1} for IFR2, FD, and CMOD4 data, respectively. Residuals were dependent on wind speed. IFR2 wind speeds were less (greater) than IMET for speeds below (above) 8 m s^{-1} (Figure 2A); this behavior was different than that reported by *Graber et al. [1996],* in which IFR (an early version of IFR2) underestimated buoy observations for wind speeds from 5- 15 m S-l. The dynamic range of each ERS-1 collocated data set exceeded that of the IMET data. Slopes of the orthogonal regression line computed between IMET minus ERS- 1 wind speed residuals and IMET wind speed were -0.1, -0.2, and -0.4 for CMOD4, IFR2, and FD data, respectively. The slopes -0.1 for CMOD4 and -0.2 for IFR2 were not statistically different at the 95% confidence level. Root-mean-square (rms) difference between I MET and IFR2 wind speeds was 0.8 m s^{-1}, which was equal to that computed

with CMOD4 data and which was 0.S m s^{-1} smaller compared to FD. The 0.5 m S-l rms difference was significant at the 95% confidence level.

There were 43 collocations with I MET directions between 0° and 100°, and 31 match ups between 210° and 310° (Figure 2B). Wind direction is defined to be the direction from which the wind was blowing. During the northeast monsoon, mean (standard deviation) values of the collocated IMET minus ERS- 1 wind direction residuals were 2 (13), 2 (11), and 4 (24) for IFR2, CMOD4, and FD, respectively. During southwest monsoon conditions, mean (standard deviation) values of the collocated IMET minus ERS-1 wind direction residuals were 9 (8), 9 (11), and 10 (7) degrees for IFR2, CMOD4, and FD, respectively. It is noted that *Large et al.* [1995] found negligible biases in the directions of altitude-corrected wind directions computed from low-level buoy data.

It is not surprising that IFR2 data were more representative of IMET observations. The σ_0 to wind speed and direction model function for IFR2, unlike those for CMOD4 and FD, was created with moored buoy wind data in the North Atlantic and North Pacific during .1992. Biases such as that identified by *Large et al. [1995]* could therefore be inherent in the IFR2 model, and would not be identified by additional buoy comparisons. The IFR2 data were the ERS- 1 vector data most consistent with IMET measurements. However, we can not equivocally state that IFR2 data are the most accurate of the three ERS-1 data products.

)9 Although IFR2 data are analyzed below and were the ERS- 1 vector wind data most consistent with IMET measurements, we can not unequivocally state that IFR2 data are the most accurate of the three ERS-1 data products.

3. Arabian Sea Surface Wind Stress Field

Wind stress components, τ_x (positive eastward) and τ_y (positive northward), are defined by

$$\tau_x = \rho_a \, CD \, u \, (U^2 + v^2)^{1/2} \qquad \text{(1a)}$$

and

$$\tau_y = \rho_a \, CD \, v \, (U^2 + v^2)^{1/2}, \qquad \text{(1b)}$$

where ρ_a is air density (1 .225 kg m^{-3}) and C_D is a non-dimensional drag coefficient. We used a 10-m height wind-speed dependent CD [*Trenberth et al.*, 1990]. τ_x and τ_y were computed from 1-day average *u* and v in 1/3° x 1/3° areas. All 1/3° x 1/3° daily τ_x and τ_y value in 1° x 10 regions were averaged to monthly mean τ_x and τ_y, from which monthly mean wind stress magnitude, $\tau = (\tau_x^2 + \tau_y^2)^{1/2}$, and direction, $\phi = \tan^{-1}(\tau_x /Q$, were calculated.

3.1. Seasonal Cycle

In January 1995 (Figure 3A), the dominant wind directions were northerly off India and northeasterly in the western Arabian Sea. The directions were representative of northeast trade winds which are found throughout the year at similar latitudes in the Atlantic and Pacific. Wind stress decreased from west to east, and near India wind stresses were two-thirds as large as those in the western Arabian Sea.

In July 1995 (Figure 3C) the wind stress field was remarkably different than January, with southwesterly (westerly) direction over the western (eastern) Arabian Sea and much larger wind stresses. In July, virtually the entire Arabian Sea had wind stresses greater than 0.1 $N m^{-2}$, which in January occurred only over a small region near Somalia. The Somali Jet entered the North Indian Ocean at the Somalia coast near 5“N, rapidly gaining strength as it penetrated towards the northeast. Maximum intensity (0.33 N m^{-2}) occurred about 200 km offshore of Somalia at 9.5°N, 53.5°E where some of the strongest (July 1995 mean wind speed was 14 m s^{-1}) and steadiest winds occur in the world during northern summer. The area oft > 0.2 N m^{-2} extended downwind towards the northeast for more than 1000 km, covering a large portion of the basin. Assuming that patches of $\tau > 0.3$ N m^{-2}, of which three occurred in July 1995, are within the Somali Jet, then in the western Arabian Sea the jet trajectory is easily defined: from Somalia at 5°N to 10°N, 53°E to 12°N, 57°E to 13“N, 61 ‘E. East of 61 “E, the Somali Jet diminished in strength. Using directions of high wind stresses as a guide, the Somali Jet entered India at 20°N. This pattern resembled one branch of the split Somali Jet portrayed by *Findlater [1971*] who analyzed l-km height winds. A split Somali Jet did not appear in the IFR2 wind pattern for July 1992, 1993 and 1994. *Findlater*

[1971] had inferred a split Somali Jet from very sparse wind observations at l-km altitude with no data in the 5- 15°N, 53- 73°E area. Whether the Somali Jet has one or two branches is a subject of continuing debate [P. Webster, personal communication, 1997].

Whether the number of intense wind stress patches along the Somali Jet was dependent on the ERS - 1 sampling scheme was investigated with ECMWF winds, which are produced at 1.125°-latitude x 1.1250-longitude resolution every six hours. ECMWF winds yielded a single patch near Somalia. ECMWF winds subsampled with the ERS - 1 sampling scheme yielded two patches, indicating that ERS - 1 sampling produced one or more spurious patches of intense wind stress. A future study of Somali Jet patchiness will be made with surface wind velocity data from the National Aeronautics and Space Administration (NASA) scatterometer (NSCAT), which was launched in August 1996 and which provides twice the quantity of data because it is a double-swath scatterometer.

April 1995 (Figure 3B) was associated with calm conditions. The October 1995 (Figure 3D) wind stress field was similar to that in April, both representing transitions between monsoons.

3.2. Monsoon Onset

Throughout India, the time of monsoon onset is easily defined as the day when it begins to rain and continues to rain heavily for 1-2 weeks, before a break in the monsoon appears. Rainfall is not a good indicator of monsoon conditions over the Arabian Sea because there is not much rainfall, especially in the western area where hardly any rain occurs. IMET rainfall measurements totaled 5 cm from October 1994 to October 1995 [Weller, 1996].

For ocean circulation studies, we define the start of the southwest monsoon at a specific location to be the beginning of the initial interval in Mayor June of sustained wind velocities having eastward and northward components and having a speed greater than 7.5 m S-l. These conditions must persist for at least 6 consecutive days, which is 3 inertial periods at 15°N and 2 inertial periods at 10°N and which is considered to be a minimum time to generate Ekman currents. The choice of 7.5 m s^{-1} seems reasonable because the global mean wind speed over the ocean is

about 7.5 m S-*, and monsoon wind speeds are known to be above average. With this definition of monsoon onset time, the start of the 1995 monsoon at IMET was 6-7 June (Figure 4).

IFR2 wind velocities recorded within the 10x 10 area centered at IMET yielded 6-7 June (with no data recorded from 29 May -5 June) as the time of monsoon onset (Figure 4). The excellent agreement between IFR2 and IMET times of monsoon onset provides an opportunity to examine the monsoon onset at the IMET location in other years when no IMET was there. For 1992, 1993, and 1994, the times of monsoon-wind onset were 14-15 June, 16-17 June (with no data from 8-15 June), and 10-11 June (with no data from 6-9 June), respectively. Onset times were consistent with the 11 - 12 June (with a 30-day standard deviation) climatological-mean onset time of monsoon rainfall on the west coast of India near 20°N [*Dhar et al.*, **1980].** At IMET (15.5°N, 61 .5°E), the range of monsoon onset time for 1992-1995 was 10 days.

Onset times at the 9.5°N, 53.5°E site of maximum wind stress, named Site T, were 14-15 June 1992,29-30 May 1993,31 May -1 June 1994, and 8-9 June 1995. The range was 16 days. Comparing onset times at T and IMET indicated considerable geographical variation. The influence of ERS - 1 sampling [*Zeng and Levy*, 1995] on spatial features of monsoon onset time will be examined with NSCAT data.

4. Wind-Driven Ocean Transports

4.1. Background

Assuming the monthly mean vertical velocity at the sea surface is zero, the horizontal divergence of the Ekman wind drift is equal to ρw_E, where p is sea-water density (1 025 kg m^{-3}) and w_E is the vertical velocity at the bottom of the Ekman layer. According to *Stommel [1965]*,

$$w_E = (1/\rho f)(\mathrm{curl}_z \tau + \beta \tau_x / f). \qquad (2)$$

The Coriolis parameter, f, is equal to $2\Omega \sin\vartheta$, ϑ is the latitude, Ω is the rotation rate of the earth (7.29 x10-S rad S-l), and β, the rate of change of the Coriolis parameter with latitude, is equal to $2\Omega \cos\vartheta / R$ with R equal to the radius of the earth (6.37x 10^6 m). Curlzz, the vertical component of wind-stress curl, is defined by

$$curl_z\tau = \partial\tau_y/\partial x - \partial\tau_x/\partial y = \Delta\tau_y/\Delta x - \Delta\tau_x/\Delta y. \quad (3)$$

$Curl_z\tau$ was computed from monthly mean 10x 10 τ_x and τ_y values.

The meridional Ekman transport per unit zonal width is $-\tau_x/\rho f$ [*Stommel*, 1965]. The vertically integrated north-south geostrophic and Ekrnan transports per unit zonal width, named Sverdrup transport, is $curl_z\tau/\rho\beta$ [*Stommel*, 1965].

The Arabian Sea is considered to be a closed basin, with boundaries along 8"N, 24°N, 50"E and 77°E (Figure 1). Employing conservation of mass, a lowest-order approximation of wind-driven circulation in the Arabian Sea during the southwest monsoon consists of water upwelling into the Ekman layer, water exiting the Arabian Sea along 8.5°N, and water entering the Arabian Sea by the Somali Current. In this scenario, the Somali Current transport would equal the Sverdrup transport: this simple view is contrary to the idea that the Somali Current is largely the coastal manifestation of the Great Whirl. The total upward transport into the Ekman layer is assumed to exit the Arabian Sea in the Ekman layer. Over the interior of the Arabian Sea the upward transport computed from wind stress curl is expected to be smaller than the Ekman transport across 8.5°N because two additional sources of water entering the Ekman layer are coastal upwelling and Somali Current. Because land contaminates the σ_0 from the ocean, no estimate of coastal upwelling is made. Hereafter, vertical transport across the bottom of the Ekman layer over the Arabian Sea excludes transport within a 50-km coastal zone.

4.2. **Monthly Mean Ocean Transports, 1992 - 1996**

Monthly mean vertical transport across the bottom of the Ekman layer of the Arabian Sea north of 8°N, meridional Ekman transport along 8.5"N, and Sverdrup transport along 8.5° were computed from May 1992- May 1996 (Figure 5). Time series began in May 1992 because final calibration of σ_0 was made in March 1992 and wind coverage in April 1992 was poor because the ERS- 1 orbit was dedicated to a non-oceanographic objective.

4.2.1. Comparison **With In Situ Data.** *Chereskin et al. [1997]* computed wind-driven upper ocean transports along 8.5°N from acoustic Doppler current profiler (ADCP)

measurements recorded from research vessels Malcolm *Baldridge* and *Knorr* during 4- 12 June 1995 and 13 - 26 September 1995, respective y. *Malcolm Baldridge* measurements did not extend east of 70°E. ADCP estimates of wind-driven southward transport in June and September were -18 and -8 Sv, respectively. IFR2 southward Ekman transports across 8.5°N for 4-12 June and 13-26 September 1995 were -15 and -6, respectively. The 4-12 June to 13-26 September ratio of ADCP wind-driven transports was nearly the same as that determined from IFR2 Ekman transports, which is an encouraging sign about reliability of IFR2 Ekman transport. The larger magnitudes associated with the ADCP method could be related to the Great Whirl, a non wind-driven feature which would create southward flow near 55°E.

A presumed equivalence between Somali Current transport and Sverdrup transport at the same latitude suggests a test about the representativeness of IFR2 Sverdrup transport. During 3-4 June and 12-13 September 1995, *Malcolm Baldrige* and *Knorr*, respectively, recorded ADCP measurements across the Somali Current near 9°N. D. Wilson (personal communication, 1996) and T. Chereskin (personal communication, 1996) computed Somali Current transports over the uppermost 450 m of 17 and 24 Sv in June and September, respectively, which included estimates of the current over the continental shelf where no ADCP data were recorded. IFR2 Sverdrup transports along the Arabian Sea southern boundary at 8.5°N were not calculated for 3-4 June and 12-13 September 1995 because of poor data coverage. IFR2 Sverdrup transports along 8.5°N for 4-12 June and 13-26 September 1995 were 3 and -8 Sv, respectively; however these values are not reliable because of large variations of zonal averaged IFR2 transports at 1 ‘-latitude intervals. In addition to inadequate ERS - 1 sampling during a 12-day interval, another reason for employing a longer averaging time to compute the Sverdrup transport is that the Sverdrup transport is applicable to steady state motion or for motion with long-period variations, such as 10 inertial periods. Monthly mean zonal averaged IFR2 Sverdrup transport varied smoothly with latitude. Thus, monthly mean IFR2 Sverdrup transport values are compared to Somali Current transport. IFR2 Sverdrup transports along the Arabian Sea southern boundary at 8.5°N for June and September 1995 were -8 and -12 SV, respectively (Figure 5), which were one-half the magnitude of the

measured Somali Current transport. The June-to- September rat ios of ADCP Somali Current transports and IFR2 Sverdrup transports were almost the same. The difference between Somali Current transport and Sverdrup transport could be related to the Great Whirl, which would enhance Somali Current transport.

4.2.2. **Seasonal Cycle.** Four-year (June 1992- May 1996) mean values of vertical transport at the bottom of the Ekman layer over the Arabian Sea (excluding a 50-km wide coastal zone), meridional Ekman transport along the Arabian Sea southern boundary at 8.5°N, and Sverdrup transport along the Arabian Sea southern boundary at 8.5°N were -0.5,-2.7, and -4.0 Sv, respectively. For each variable, month-to-month variations were similar for each year (Figure 5) and the ranges of four 1-year mean values were smaller than 1 Sv.

Caution is advised in interpretation of vertical transport over the Arabian Seato be representative of vertical motion throughout the Arabian Sea. The Somali Jet strongly influences the spatial distribution of wind-stress curl. During summer monsoon, water sinks (rises) in the southern (northern) portion of the Arabian Sea (Figure 6).

Transports during monsoons were substantially greater than the annual mean (Figure 5). At the beginning of the southwest monsoon, water is upwelled into the surface layer. A break in upwelling in August - September occurred in three of four years; the exception occurred in 1994. During the 1992-1995 June - September monsoon, the average volume of water upwelling into the Ekman layer (3.4 Sv) was about one-third smaller than that exiting in the Ekman layer across the Arabian Sea southern boundary at 8.5°N. Additional waters for the Ekman layer are the Somali Current, in which the surface current reaches 1 m s-], and coastal upwelling off Oman [*Smith and Bottero, 1977]. The 1992-1995* June - September mean Sverdrup transport along the Arabian Sea southern boundary at 8.5°N was 15 Sv, and year-to-year variability was very small (0.3 Sv).

During the 1992-1996 December - March monsoon, the average amount of northward-flowing water in the Ekman layer at the Arabian Sea southern boundary was 3.8 Sv (Figure 5), which was 1 Sv or 20% less than that downwelled through the bottom of the Ekman layer over the Arabian Sea. The 1 Sv imbalance is consistent with 5 Sv equatorward flow along east Africa

[*Bruce et* al., 1994], 7 Sv poleward flow off west India [*Shetye et* al., 1991], and a 0.3 Sv Sverdrup transport along 8.5°N (Figure 5).

In three of four years, the maximum southward Sverdrup transport occurred in July, which was about one month after the time of the maximum southward Ekman transport (Figure 5). This is consistent with different spin-up times for Ekman and Sverdrup transports. Spin-up times will be analyzed with NSCAT data because of the greatly increased daily coverage.

5. Concluding Remarks

Three ERS-1 surface wind velocity data products were examined over the Arabian Sea where large wind speeds and large gradients of wind components exist. Comparison of IMET and ERS-1 data during October 1994 to October 1995 revealed that the IFR2 data product was more representative of IMET observations than CMOD4 and FD data. The three ERS-1 data sets differed in the formulation of the model function and in the ambiguity removal algorithm. Perfect agreement between IMET and IFR2 data can not be achieved because a time-averaged buoy wind measurement is not compatible with a near-instantaneous areal-averaged satellite wind measurement, even if no errors were associated with each measurement. This fundamental incompatibility, as well as collocation errors and random errors in the scatterometer data can lead to apparent systematic biases, especially in wind speed comparisons, if the buoy measurements are assumed to be error-free [*Freilich*, 1997]. Reliability y of IFR2 data was further enhanced by the good correspondence between IFR2 Ekman transports and ADCP wind-driven upper ocean transports. Agreement between variations of measured Somali Current transport and computed Sverdrup transport along the Arabian Sea southern boundary at 8.5°N in June and September 1995 suggests that the Sverdrup transport along the Arabian Sea southern boundary has merit to be a Somali Current transport index, which requires further evaluation. IFR2 Sverdrup transport should be compared with that simulated from an ocean general circulation model (OGCM) and with OGCM simulations of Somali Current transport.

IFR2 data did not portray a split Somali Jet, unlike that described by *Findlater* [1971]. Wind vectors at the surface are not the same as at 1-km altitude because wind direction rotates with height in the tropical planetary boundary layer. The difference of the Somali Jet at the surface and aloft is a subject for further investigation.

A remarkable feature of the Arabian Sea is that sea surface temperature in July is 2 “C lower than in April, and in July sea surface temperature is almost as low as that in January. This atypical behavior for northern latitudes in summer is caused by extreme ocean-atmosphere interactions during the southwest monsoon. Understanding the relative importance of several physical processes, such as evaporation, entrainment, upwelling, and horizontal advection, requires accurate knowledge of surface winds. Aliasing will be substantially reduced with NSCAT data. Because no single data source can capture the rich spectrum of surface winds, research is warranted on integration of ERS-2 (ERS - 1 follow-on) and NSCAT data with in situ data.

Acknowledgements. We are grateful to Dr. Teresa Chereskin (Scripps Institution of Oceanography) and Douglas Wilson (NOAA Atlantic Oceanographic and Meteorological Laboratories) for kindly sending *Knorr* and *Malcolm Baldridge* results in advance of their publication. Dr. Kenneth Brink (Woods Hole Oceanographic Institution) and Dr. Robert Knox (Scripps Institution of Oceanography) provided valuable comments on an early version of the manuscript. Computer-generated data processing and graphical/tabular analyses were made by Peter Woiceshyn (JPL) in an outstanding manner. The work described in this paper was supported by the NASA Physical Oceanography Program RTOP 622-47-09; NASA SeaWinds Project RTOP 229-18-41 (DH); NASA NSCAT Project via JPL contract 959351 (MlIF); and ONR grant N0001 4-94-1-0161 (RW). The research described in this paper was performed, in part, by the Jet Propulsion Laboratory, California Institute of Technology, under contract with the National Aeronautics and Space Administration.

References

Attema, E. P. W., The active microwave instrument on board the ERS-1 satellite. *Proc. IEEE, 79, 791-799, 1991.*

Bruce, J. G., D. R. Johnson, and J. C. Kindle, Evidence for eddy formation in the eastern Arabian Sea during the northeast monsoon. *J. Geophys. Res.*, 99, 7651-7664, 1994.

Chereskin, T. K., W. D. Wilson, H. L. Bryden, A. Ffield, and J. Morrison, Observations of the Ekman balance in the Arabian Sea during the 1995 southwest monsoon. *Geophys. Res. Letts.*, in press, 1997.

Dhar, O. N., P. Rakhecha, and B. Mandal, Does early or late onset of monsoon provide any clue to subsequent rainfall during the monsoon season? *Mon. Wea. Rev., 108, 1069-1072, 1980.*

Findlater, J., Mean monthly air flow at low levels over the western Indian Ocean. *Geophys. Mem., No.* 115, H. M. S. O., London, 53 pp., 1971.

Freilich, M. H., Validation of vector magnitude data sets: Effects of random component errors. *J. Atmos. Oceanic Tech., 14,695-703, 1997.*

Freilich, M. H., ERS - 1 scatterometer measurements over the Southern Ocean. *Proc. Second ERS-1 Sym., Space at the Service of our Environment, 11-14 October 1993, Hamburg,* European Space Agency, Paris, 1111-1116, 1994. [ISBN 92-9092-286-9]

Freilich, M. H., and R. S. Dunbar, A preliminary C-band scatterometer model function for the ERS-1 AMI instrument. *Proc. First ERS-1 Sym., Space at the Service of our Environment, 4-6 November 1992, Cannes,* European Space Agency, Paris, 79-83, 1993. [ISBN 92-9092-278-8]

Graber, H. C., N. Ebuchi, and R. Vakkayil, Evaluation of ERS - 1 scatterometer winds with wind and wave ocean buoy observations. RSMAS Tech. Rept. 96-003, Univ. Miami, 78 pp., 1996.

Knox, R. A., The Indian Ocean: Interaction with the monsoon. In, *Monsoon,* J. S. Fein and P. L. Stephens, Editors, John Wiley& Sons, 365-397, 1987.

Large, W. G., J. Morzel, and G. B. Crawford, Accounting for surface wave distortion of the marine wind profile in low-level Ocean Storms wind measurements. *J. Phys. Oceanogr.*, *25*, 2959-2971, 1995.

Naderi, F., 'M. H. Freilich, and D. Long, Spaceborne radar measurement of wind velocity over the ocean - An overview of the NSCAT scatterometer system. *Proc. IEEE, 79,850-866, 1991.*

Offiler, D., The calibration of the ERS-1 satellite scatterometer winds. *J. Atmos. Oceanic. Tech., 11, 1002-1017, 1994.*

Quilfen, Y., and A. Bentamy, Calibration/validation of ERS-1 scatterometer precision products. *Proc. IGARSS 1994, Pasadena, 8-12 August 1994.* IEEE, Pisacataway, NJ, 945-947, 1994. [ISBN 0-7803-1497-2]

Shetye, S., A. Gouvea, S. Shenoi, G. Michael, D. Sundar, and K. Santanam, The coastal current off western India during the northeast monsoon. *Deep-Sea Res.*, *38*, 1517-1529, 1991.

Smith, R. L., and J. Bottero, On upwelling in the Arabian Sea. In, *A Voyage of Discovery, George Deacon 70th Anniversary Volume,* M. Angel, Editor, Pergamon Press, 291-304, 1977.

Stoffelen, A. and D. Anderson, Scatterometer data interpretation: Estimation and validation of the transfer function CMOD4. *J. Geophys. Res.*, 102, 5767-5780, 1997.

Stommel, H. M., *The Gulf Stream.* University of California Press, 248 pp, 1965.

Trenberth, K. E., W. G. Large, and J. G. Olson, The mean annual cycle of the global ocean wind stress. *J. Phys. Oceanogr., 20, 1742-1760,* 1990.

Weller, R. A., In situ observations of surface meteorology and air-sea fluxes. 1996 U.S. WOCE Report, Texas A&M University, College Station, TX, 17-20, 1996.

Weller, R. A., and S. P. Anderson, Surface meteorology and air-sea fluxes in the western equatorial Pacific warm pool during the TOGA Coupled Ocean-Atmosphere Response Experiment. *J. Climate,* 9, 1959-1990, 1996.

Zeng, L., and G. Levy, Space and time aliasing structure in monthly mean polar-orbiting satellite data, *J. Geophys. Res., 100,* 5133-5142, 1995.

List of Figures

Figure 1. Location of WHOI moored buoy is represented by the triangle. The region defined to be the Arabian Sea is shaded.

Figure 2. Scatter diagrams of IMET - IFR2 (A) wind speed residuals and (B) wind direction residuals. Abscissas are (A) IMET wind speed and (B) IMET wind direction. Solid line in (A) is least-squares orthogonal regression line.

Figure 3. Monthly mean IFR2 wind stress magnitudes and directions during (A) January 1995, (B) April 1995, (C) July 1995, and (D) October 1995. Contour interval is 4×10^{-2} N m^{-2}. Wind stress direction was computed from monthly mean 10 x 1° τ_x and τ_y values. Arrows point in the direction the wind is blowing. Arrow length is constant. For clarity, arrows are shown for alternate lox 10 areas.

Figure 4. Time series of 2-day average wind speed computed from IMET (open circle) and IFR2 (solid dot) data. About 17 individual IFR2 wind vectors were averaged to form a 10x 1° 2-day value centered at the lMET location.

Figure 5. IFR2 monthly mean vertical transports into the Ekrnan layer of the Arabian Sea north of 8"N (dash line), north-south component of Ekman transport along 8.5°N (dotted line), and Sverdrup transport along 8.5°N (solid line). Asterisks indicate that ERS- 1 data coverage in January, February and March 1994 was about 50% less compared to other months.

Figure 6. Vertical velocity at the bottom of the Ekman layer per lo-longitude x lo-latitude regions computed from IFR2 winds for July 1995. Contour interval is 10x10-6 m S-l. Shaded region represents downwelling.

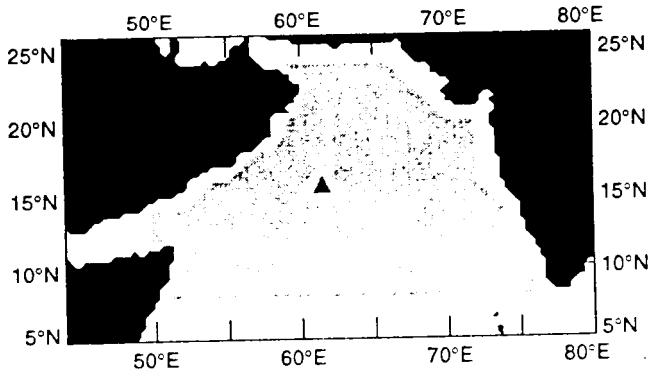

Figure 1

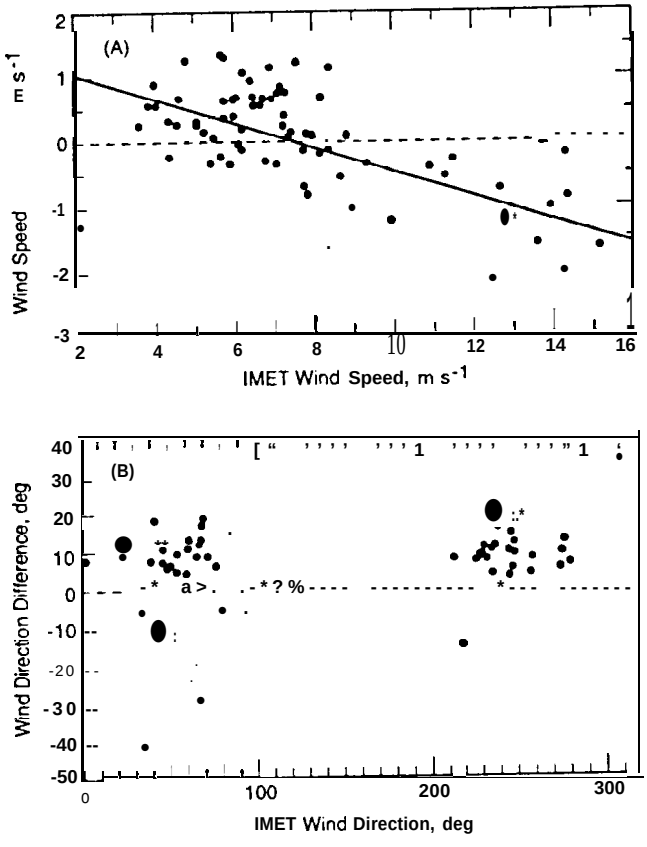
(A)
Wind Speed
IMET Wind Speed, m s-1
(B)
Wind Direction Difference, deg
IMET Wind Direction, deg

Figure 2

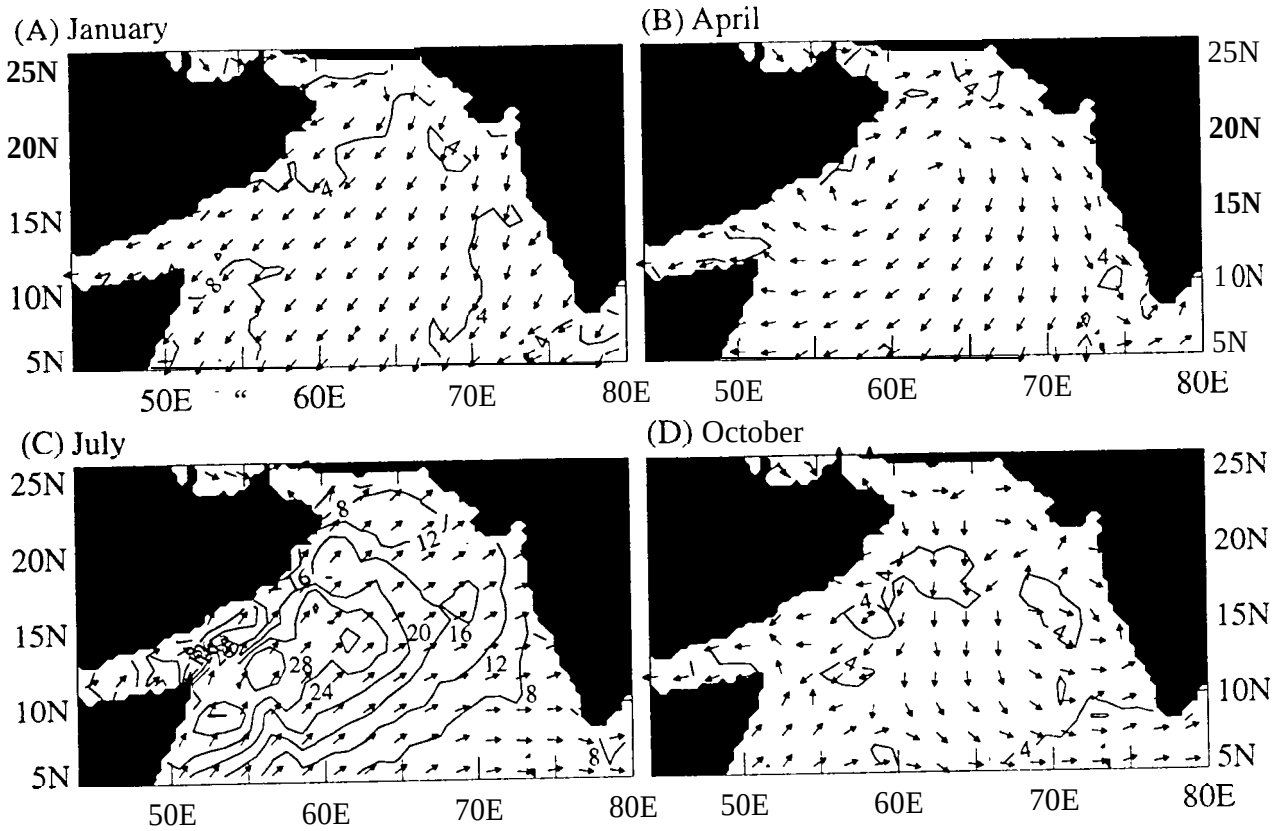
(A) January
(B) April
(C) July
(D) October
25N
20N
15N
10N
5N
50E
60E
70E
80E

Figure 3

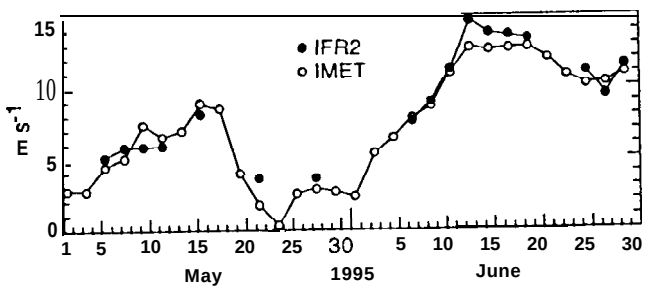
15
10
5
0
E s-1
IFR2
IMET
1
5
10
15
20
25
30
5
10
15
20
25
30
May
1995
June

Figure 4

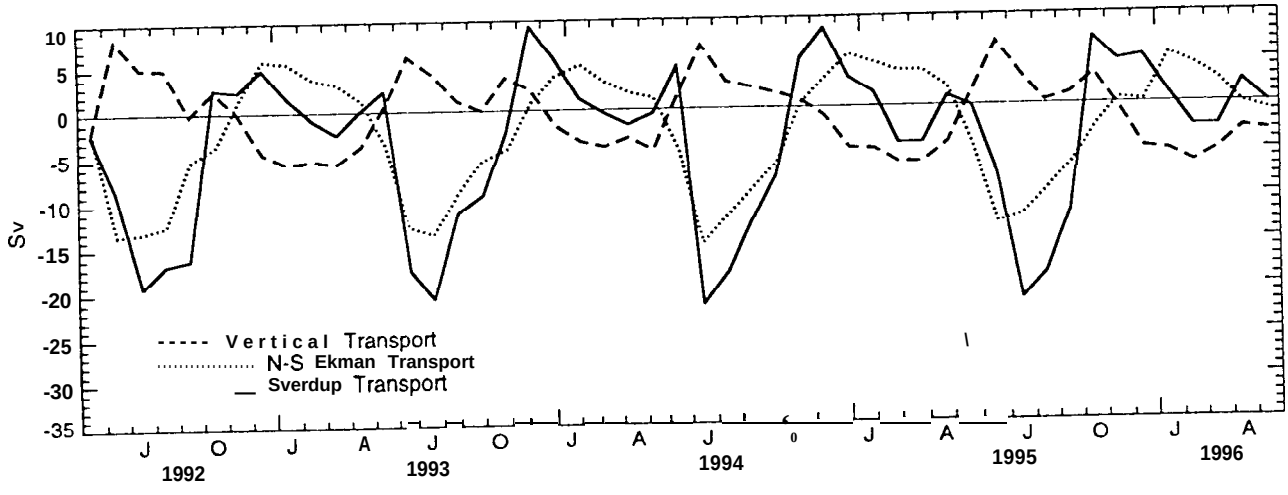
10
5
0
-5
-10
-15
-20
-25
-30
-35
Sv
Vertical Transport
N-S Ekman Transport
Sverdup Transport
J O J A J O J A J O J A J O J A
1992
1993
1994
1995
1996

Figure 5

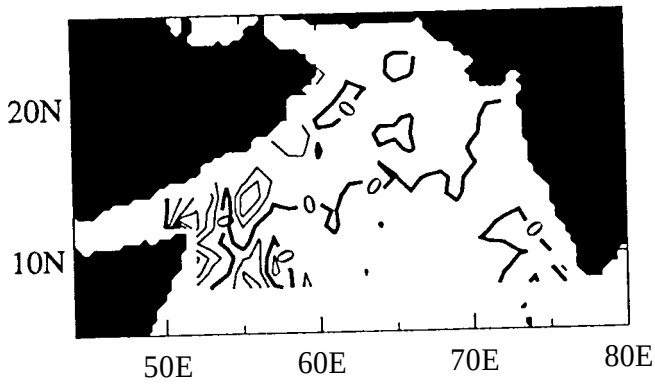

Figure 6